THE JOURNAL OF PHYSICAL CHEMISTRY C
A JOURNAL OF THE AMERICAN CHEMICAL SOCIETY

pubs.acs.org/JPCC

Article

Zeolite Phase Selectivity Using the Same Organic Structure-Directing Agent in Fluoride and Hydroxide Media

Santiago Leon and German Sastre*

Cite This: J. Phys. Chem. C 2022, 126, 2078−2087

Read Online

ACCESS | Metrics & More | Article Recommendations | Supporting Information

ABSTRACT: Force field-based calculations of all-silica zeolites show the role of fluoride as a structure-directing agent (SDA). Calculations of fully packed organic and fluoride SDAs were possible with an updated version of zeoTsda software, based on Monte Carlo+Lattice Energy Minimization. Comparison between fluoride-containing and fluoride-free calculations using the same organic SDA allowed us to predict which zeolite phase is obtained in fluoride and hydroxide media and also, through a new energy decomposition scheme, identify energetic contributions driving the synthesis outcome.

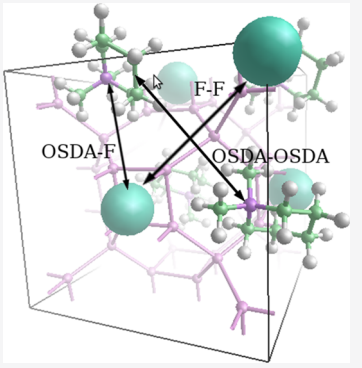

1. INTRODUCTION

Zeolites are a large and growing family of currently 255 microporous crystalline aluminosilicates, aluminophosphates, and their chemically related derivatives, formed by corner-sharing tetrahedral frameworks, which find applications in catalysis and separation industrial processes.

Two important hydrothermal synthetic routes differ in using either a hydroxide or a fluoride anion as a mineralizer, influencing the final microporous material obtained. The incorporation of each anion in the zeolite framework has utterly different effects. While hydroxide gives internal silanol nests leading to connectivity defects, fluoride is incorporated inside small cavities, giving defectless structures.

Flanigen and Patton introduced the fluoride route[1] and noted that (a) it increases the solubility of silica species at neutral pH and (b) catalyzes the condensation reactions making Si−O−Si bonds; hence, the fluoride route is particularly successful in obtaining all-silica zeolites. A third aspect of the fluoride route is the structure-directing effect of fluoride, which always acts jointly to that of the organic structure-directing agent (OSDA), and hence, it is not easy to separate both effects. This will be attempted in the present study.

The fluoride route remains academically important, since it contributes to the synthesis of new structures and to understanding better the outcomes and intricacies of the zeolite synthesis, but the inherent danger and environmental disadvantage of using HF makes this route commercially inconvenient. In just a few cases, structures first synthesized in fluoride were later synthesized in hydroxide media, such as BEC (silicogermanate),[2] ITQ-21 (silicogermanate),[3] STF (pure silica),[4] IWV (aluminosilicate),[5] SVR (aluminosilicate[6] and pure silica[7]), and STW (pure silica),[8] this being a two-step process that may allow introduction of new zeolites in industrial applications, through the more environmentally safe synthesis in hydroxide media.

Examples of all-silica zeolites synthesized in hydroxide media, apart from the two above-mentioned ones (STF and STW), are DDR,[9] MRE,[10] CFI,[11] MWW,[12] AFI,[13] STO,[14] PCS,[15] RRO,[16] and SFV.[17] We estimate that at least 50 topologies can be synthesized as all-silica in hydroxide media. The total number of all-silica structures is 68,[18] and they are indicated in Table S1.

The number of all-silica zeolites has grown considerably, since the fluoride route has been employed by an increasing number of research groups. Table 1 of a study by Lu et al.[19] includes 22 structures obtained for the first time as all-silica using the fluoride route. The latest three obtained are STW, *-SSO, and CSV. Recent new topologies first obtained as all-silica in hydroxide media are IFY, EWT, SVY, and PCS.

An important observation is that structures containing a small cage formed by eight tetrahedral atoms, named [4^6] or double four ring (D4R), can be synthesized more easily using fluoride rather than hydroxide media.[20] More in general, it can be said that fluoride favors the formation of small cavities

Received: October 4, 2021
Revised: January 11, 2022
Published: January 23, 2022

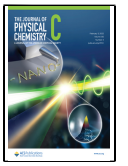

Table 1. Selection of Full Results from Tables S1 and S2 and Total Energy and Contributions (eV/SiO_2) of Zeo−OSDA Systems in the Presence (F) and Absence (noF) of Fluoride[a]

			F	noF	(4)	(7)	(9) F	(9) noF	(10) F	(10) noF
z-SDA	nSi	nSDA	$E(T)$	$E(T)$	E(SDAF) (cou)	E(z-SDAF) (cou)	E(z-SDA) (vdw)	E(z-SDA) (vdw)	E(z-SDA) (vdw/SDA)	E(z-SDA) (vdw/SDA)
sda01_AST	40	4	−41.116	−40.571	−0.380	−0.553	−0.106	−0.109	−1.061	−1.085
sda01_NON	88	4	−40.645	−40.572	−0.151	−0.189	−0.044	−0.046	−0.974	−1.011
sda02_MEL	96	4	−40.754	−40.557	−0.115	−0.225	−0.041	−0.039	−0.979	−0.946
sda02_MTW	56	2	−40.736	−40.577	−0.110	−0.152	−0.039	−0.039	−1.087	−1.102
sda03_STF	64	4	−40.736	−40.491	−0.175	−0.314	−0.076	−0.073	−1.217	−1.161
sda03_STO	112	4	−40.651	−40.543	−0.067	−0.204	−0.037	−0.039	−1.049	−1.084
sda04_STF	64	4	−40.782	−40.512	−0.173	−0.313	−0.064	−0.069	−1.029	−1.106
sda04_STO	224	8	−40.693	−40.562	−0.094	−0.189	−0.033	−0.037	−0.917	−1.027
sda05_CON	56	2	−40.642	−40.502	−0.090	−0.189	−0.035	−0.033	−0.988	−0.931
sda05_NES	136	6	−40.688	−40.522	−0.124	−0.262	−0.049	−0.053	−1.110	−1.195
sda05_STF	64	4	−40.775	−40.513	−0.163	−0.320	−0.073	−0.075	−1.168	−1.194
sda05_STO	224	8	−40.695	−40.563	−0.090	−0.190	−0.038	−0.040	−1.059	−1.113
sda06_DOH	34	1	−40.670	−40.554	−0.086	−0.107	−0.035	−0.035	−1.190	−1.193
sda06_STO	112	3	−40.668	−40.567	−0.058	−0.152	−0.025	−0.025	−0.946	−0.948
sda07_CHA	36	3	−40.871	−40.501	−0.276	−0.325	−0.114	−0.115	−1.374	−1.375
sda07_MWW	72	4	−40.662	−40.445	−0.138	−0.291	−0.047	−0.049	−0.839	−0.887
sda08_LTA	24	2	−40.550	−40.344	−0.265	−0.550	−0.084	−0.089	−1.011	−1.072
sda08_UFI	64	4	−40.515	−40.407	−0.173	−0.365	−0.073	−0.071	−1.170	−1.131

[a]"nSi" is the number of SiO_2 in the unit cell; "nSDA" is the number of OSDA molecules in the unit cell. Number code of the energy contributions given in Section S2.

containing 4-rings[21] and in particular D4Rs. In the present work, the only zeolites with D4Rs are AST, LTA, and UFI.

From the total of 41 structures containing D4R, 9 have been obtained as pure silica using the fluoride route: AST, ISV, ITW, BEC, ITH, STW, LTA, IHW, and IWR. These pure silica structures cannot be, as far as we know, obtained in hydroxide media, except STW.[8] Also, pure silica structures without D4R can be obtained in fluoride media, such as BEA, ITE, IFR, CHA, STF, MTF, ATS, -ITN, RTH, NES, EUO, CON, SAS, and -SVR.

Figure 3 of the study by Lu et al.[19] shows a large increase in the number of new structures containing D4Rs that were synthesized, since the fluoride route became widely used. This happened after 1998, when Villaescusa, Camblor, and co-workers made the breakthrough discovery of using the water/silica ratio as a new synthesis variable within the fluoride route, leading to the formation of less-dense structures as the gels become more concentrated.[22]

Liu et al.[23] explained this effect using all-silica ITQ-13 (ITH), with fluoride located both in $[4^15^26^2]$ and D4R cavities. While in the first cavities, fluoride could be exchanged by SiO^- defects, mainly, stabilized at 6-rings, this was not possible with fluorides in D4Rs, hence the current impossibility to synthesize all-silica ITH in the absence of fluoride.

The rule of fluoride media favoring the presence of 4-rings and in particular D4Rs is extended and generalized when germania alone or with silica, instead of pure silica, is used as the synthesis gel in which case the number of new structures containing D4Rs is even larger. From the 25 germanates and silicogermanates (Table S2), only one of them (ECNU-21, EWO) does not contain D4Rs. A number of them were synthesized without using the fluoride route. IWW is an example, being a new structure obtained as silicogermanate, containing D4Rs, and synthesized in fluoride-free media.[24] This means that the presence of Ge is so strong in directing toward D4R-containing structures that fluoride is not mandatory. Contrarily, when the gel is pure silica, the presence of fluoride is very much needed in order to obtain structures with D4Rs.

Prior to the discovery of the fluoride route, organic molecules were identified by Barrer as SDAs in the early 1960s by roles in between a simple pore filling or a full templating effect.[25] Unlike fluoride, OSDAs show a fit (shape and size) between the OSDA and the micropore that facilitates a quantitative interpretation by simple computational chemistry calculations of the zeo−OSDA energetic interaction.[26]

An experimental and computational study by Zones and co-workers[27] using a series of piperidinium-based (with names G11−G213) OSDAs and synthesized in fluoride and hydroxide media allows one to compare the strength of the OSDA-directing effect. Correct predictions of zeolites obtained in fluoride media were AST, using G11 and G74 OSDAs (Tables 4 and 5 in ref 27); SGT using G80 (Tables 4 and 6 in ref 27); and STF using G39, G61, and G77 (Tables 4 and 6 in ref 27). Other predictions were not correct, such as AST using G210 (instead of NON, Tables 4 and 5 in ref 27) and SGT using G65 (instead of DOH, Tables 4 and 6 in ref 27).

In our own studies, it was possible to explain the different outcome of ZSM-12 (MTW) and EU-1 (EUO) structures synthesized with N-cyclohexyl-*N*-methyl-pyrrolidinium as the OSDA at lower and larger aluminum contents, respectively, with the help of a theoretical and computational model including the role of OSDAs and fluoride.[28] We also calculated the preference of OSDAs in the competing synthesis of Beta-C (BEC) and ITQ-7 (ISV) zeolites, with 1,3,3-trimethyl-6-azonium-tricyclo[3.2.1.4.6.6]-dodecane hydroxide and 1-isopropyl-4,4,7-trimethyl-4-azonia-tricyclo[5.2.2.0]-undecane-8-ene iodide giving ITQ-7 in a wide range of compositions, while OSDAs 4,4-dimethyl-4-azonia-tricyclo[5.2.2.0]-undecane-8-ene iodide and benzyl-DABCO give preferentially Beta-C.[29] Hence, computational studies can explain and predict preferential OSDA stabilities and their subsequent zeolite

https://doi.org/10.1021/acs.jpcc.1c08688
J. Phys. Chem. C 2022, 126, 2078−2087

phase selectivity, as demonstrated in a large number of studies in the past decades.[30−38]

The present study aims to assess separately the contributions of OSDAs and fluoride in the synthesis of specific zeolites. For this task, OSDAs leading to different zeolites in fluoride and hydroxide media will be selected and a new updated and complete analysis of the different energetic contributions will be presented and employed.

2. COMPUTATIONAL MODELS AND METHODS

2.1. Energy Decomposition Analysis. A new and full energy decomposition analysis has been included by taking into account all contributions to the total energy of the systems, with and without fluoride. Some previous studies taking into account the thermodynamic aspects of the synthesis of zeolites as well as a rough estimation of some aspects related to the kinetics have been presented.[28] In the present work, we start with the fluoride-containing systems and with the following expression for the full energy of the zeo−OSDA−F system:

$$E(T) = E_{zeo} + E_{zeo-OSDA} + E_{zeo-F} + E_{OSDA-OSDA} + E_{OSDA-F} + E_{F-F} + E_{OSDA} \quad (1a)$$

Equation 1a contains all the energetic terms, but some terms cannot be calculated because they involve non-neutral unit cells. For instance, the calculation of $E_{F\text{-}F}$ would imply a unit cell with only the fluoride anions, hence with nonzero (negative) charge and hence not possible to calculate. The same happens to $E_{zeo\text{-}OSDA}$, E_{OSDA}, and $E_{OSDA\text{-}OSDA}$. A solution is to regroup terms as follows:

$$E(T) = E_{zeo} + E_{OSDAF} + E_{zeo-OSDAF} \quad (1b)$$

$$E_{OSDAF} = E_{OSDAF}^{Coul-inter} + E_{OSDA}^{Coul-intra} + E_{OSDA-OSDA}^{vdw} + E_{OSDA-F}^{vdw} + E_{F-F}^{vdw} + E_{OSDA}^{vdw} + E_{OSDA}^{bond} \quad (2)$$

$$E_{zeo-OSDAF} = E_{zeo-OSDAF}^{Coul} + E_{zeo-F}^{vdw} + E_{zeo-OSDA}^{vdw} \quad (3)$$

with $E(T) = E_{zeo}$ + (2) + (3) and with specific terms that can be calculated individually, since each corresponding system is electroneutral and also because GULP allows one to decompose energy into Coulomb and van der Waals terms:

$$E_{OSDAF}^{Coul-inter} = E_{OSDA-OSDA}^{Coul-inter} + E_{OSDA-F}^{Coul-inter} + E_{F-F}^{Coul-inter} \quad (4)$$

$$E_{OSDAF}^{vdw} = E_{OSDA-OSDA}^{vdw} + E_{OSDA-F}^{vdw} + E_{F-F}^{vdw} \quad (5)$$

$$E_{OSDAF}(\text{intra}) = (2) - (4) - (5) = E_{OSDA}^{bond} + E_{OSDA}^{Coul-intra} + E_{OSDA}^{vdw-intra} \quad (6)$$

$$E_{zeo-OSDAF}^{Coul-inter} = E_{zeo-OSDA}^{Coul-inter} + E_{zeo-F}^{Coul-inter} \quad (7)$$

$$E_{zeo-F}^{vdw} \quad (8)$$

$$E_{zeo-OSDA}^{vdw} \quad (9)$$

And so, it can also be written that

$$(1a) = (1b) = E_{zeo} + (2) + (3) = E_{zeo} + (4) + (5) + (6) + (7) + (8) + (9)$$

with all the individual terms at the right-hand side being calculated and shown in Table S3. For the systems without fluoride, the equations become simpler:

$$E_{OSDA} = E_{OSDA}^{Coul-inter} + E_{OSDA}^{Coul-intra} + E_{OSDA-OSDA}^{vdw} + E_{OSDA}^{vdw} + E_{OSDA}^{bond} \quad (2a)$$

$$E_{zeo-OSDA} = E_{zeo-OSDA}^{Coul} + E_{zeo-OSDA}^{vdw} \quad (3a)$$

with $E(T) = E_{zeo}$ + (2a) + (3a) and with specific terms that will be calculated individually:

$$E_{OSDA}^{Coul-inter} = E_{OSDA-OSDA}^{Coul-inter} \quad (4a)$$

$$E_{OSDA}^{vdw} = E_{OSDA-OSDA}^{vdw} \quad (5a)$$

$$E_{OSDA}(\text{intra}) = (2) - (4) - (5) = E_{OSDA}^{bond} + E_{OSDA}^{Coul-intra} + E_{OSDA}^{vdw-intra} \quad (6a)$$

$$E_{zeo-OSDA}^{Coul-inter} \quad (7a)$$

$$E_{zeo-OSDA}^{vdw} \quad (9a)$$

The resulting expression for fluoride-free systems is, in this case,

$$E(T) = E_{zeo} + (2a) + (3a) = E_{zeo} + (4a) + (5a) + (6a) + (7a) + (9a)$$

with the results of the calculations shown in Table S4. Another term that will be calculated is the van der Wals zeo−OSDA energy per OSDA molecule, which is useful to give an idea of the relative stability of the zeo−OSDA clusters that may be formed during zeolite nucleation. The expression is, equally for fluoride and fluoride-free systems,

$$E_{zeo-OSDA}^{vdw}\left(\frac{\text{vdw}}{\text{OSDA}}\right) = \frac{E_{zeo-OSDA}^{vdw-inter}}{N_{OSDA}} \quad (10)$$

In the above equation, the van der Waals energy corresponds to all OSDAs in the unit cell, and hence, this is divided by the number of OSDAs (NOSDA) in the unit cell.

From all of the above, and in order to better understand the results and discussion below, we list below the most important energetic contributions. Unless otherwise specified, all energy contributions are divided by the number of SiO_2 in the unit cell.

$E_{\langle zeo-OSDA\rangle}^{(vdw)}$ and $E_{\langle zeo-OSDA\rangle}^{\langle vdw/OSDA\rangle}$ (see eq 9, 9a, and 10): these are the two most widely used contributions in computational studies of zeo−OSDA interactions, including the short-range van der Waals component. They are supposed to be the main contribution driving the zeolite phase outcome when OSDAs act as true templates, which happens strictly in only rare cases. The first contribution is the summation to all OSDAs in the unit cell and divided by the number of SiO_2, while the second contribution does only refer to the interaction energy per each OSDA molecule and is not included in the total energy, since the total energy is defined as divided by the number of SiO_2. The fact that these two terms are rarely dominant and hence other contributions need to be taken into account is one of the main aspects considered in this study.

E_{zeo} is the zeolite total energy divided by the number of SiO_2. When the energy of the system is minimized, the resulting zeolite geometry, without fluoride and without OSDA

https://doi.org/10.1021/acs.jpcc.1c08688
J. Phys. Chem. C 2022, 126, 2078−2087

molecules, is calculated as a single point with the optimized geometry. Hence, this does not only reflect the zeolite intrinsic stability but also takes into account any deformation that the zeolite may experience by having organic molecules occluded.

E_{OSDA}, see (6) and (6a): this is the intramolecular energy of the OSDA molecule. This reflects the deformation (strain) of the molecule to accommodate to the zeolite micropore. In the presence of fluoride, since the intramolecular energy of fluoride is zero, the term E_{OSDAF} is equivalent to E_{OSDA}.

Coulombic term E_{OSDAF}, see (4) and (4a): this includes the intermolecular electrostatic OSDA−OSDA, OSDA−F, and F−F interactions, with the two latter excluded in nonfluoride media.

Coulombic term $E_{zeo-OSDAF}$, see (3) and (3a): this includes the intermolecular electrostatic zeo−OSDA and zeo−F interactions, with the latter excluded in nonfluoride media. This contribution is supposed to be relevant only for fluoride-containing systems. In particular, zeo−F interactions will indicate the stability of fluoride in small cavities (this short-range part is only a small fraction of the total contribution), although as a Coulombic interaction it has a long-range character and it is very much related to the periodic zeolite structure.

$E_{(OSDA)}$ (intra), see (6) and (6a): this includes intramolecular terms and van der Waals and electrostatic interactions, as well as bonds, angles, and dihedrals of the OSDA. For the fluoride, being monoatomic, the contribution is zero.

2.2. Literature Search. A literature search was carried out with SciFinder,[39] leading to 157 publications on synthesis of all-silica zeolites, allowing one to pair each publication with the OSDAs employed, and classifying each as using either the fluoride or hydroxide route. Only publications and OSDAs containing at least one zeolite synthesis through either route were selected, leading finally to eight OSDA molecules and the zeolite products in fluoride (left) and hydroxide (right) media indicated in Figure 1. These are the targets that should be predicted by calculations. The names of the OSDAs, as well as their relation to the OSDAs in ref 27, and their respective CAS numbers are as follows:

Sda01 is *N*,*N*-dimethylpiperidinium (cas-15302-91-7), G11 in ref 27.

Sda02 is 1,1,3,5-tetramethyl-piperidinium (cas-146877-01-2), G24 in ref 27.

Sda03 is 6,10-dimethyl 5-azoniaspiro[4.5]decane (cas-16431-16-6), G77 in ref 27.

Sda04 is 1,1-diethyl-3-methyl-piperidinium (cas-947602-89-3), G61 in ref 27.

Sda05 is 1,1-diethyl-3,3-dimethyl-piperidinium (cas-947602-90-6), G51 in ref 27.

Sda06 is 2-ethyl-1,1-dimethyl-piperidinium (cas-244048-92-8), G65 in ref 27.

Sda07 is *N*,*N*-trimethyl-adamantammonium (cas-46244-96-6).

Sda08 is 1,2-dimethyl-3- (2-fluorobenzyl)imidazolium (cas-767624-06-6).

2.3. Finding OSDA Location in Zeolites. zeoTsda software has been updated in the present work and is now able to tackle not only neutral OSDAs in all-silica models, as in the previous version,[40] but also charged OSDAs in fluoride-containing all-silica zeolite frameworks. The software is able to automatically fill the zeolite micropores with OSDA molecules

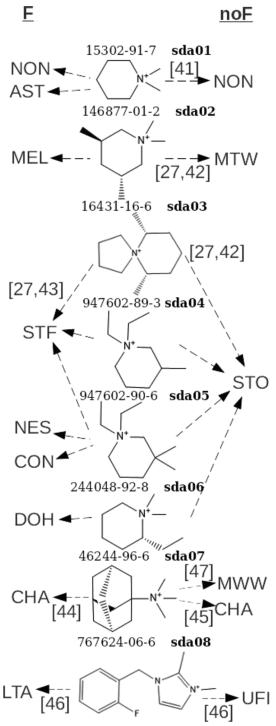

Figure 1. All-silica (or high-silica) zeolites obtained in fluoride (left) and hydroxide (right) media with common OSDAs (middle), named as sda01−sda08, and with their corresponding CAS names from the SciFinder database. Relevant references[12,27,41−46] are indicated in brackets. When not specified otherwise, the synthesis is described in ref 27.

and also to locate fluoride anions appropriately in small cavities. The only input needed from the user is the data of the zeolite unit cell and the XYZ file for the OSDA molecule. The geometries of the SDAs were optimized prior to the insertion in the Monte Carlo simulations.

Models for these zeo−OSDA systems were constructed using the all-silica unit cells obtained from the XRD data. OSDA molecules were converted from SciFinder 2-D SDF to 3-D XYZ using openbabel,[47] which also assigns atom charges and types. Fluoride and OSDAs were introduced in the zeolite unit cell up to full loading using the updated version of zeoTsda[40] presented in this study in which a new algorithm allowed the calculation of zeo−OSDA−F systems, giving the minimum energy locations of fluoride and OSDAs. For systems in hydroxide media, the approximation of using a neutralized OSDA molecule (with atomic charges different from zero but overall charge equal to zero) was employed. The calculated energies allow one to identify zeolite−OSDA phase stabilities in the presence and absence of fluoride. More details are given in the Supporting Information.

3. RESULTS

Table 1 shows the results of using LEM-MC (lattice energy minimization and Monte Carlo) in zeoTsda and the energy decomposition.

The energy decomposition allows one to (a) compare the total energies for each OSDA in zeo−OSDA systems and suggest the zeolite phase obtained with each OSDA, with and without fluoride; and (b) compare each energetic term in order to find the dominant contributions to the stability of zeo−OSDA systems in the presence and absence of fluoride. A

https://doi.org/10.1021/acs.jpcc.1c08688
J. Phys. Chem. C 2022, 126, 2078−2087

comparison with the experimental results (Figure 1) is indicated in Table 2. A general view of the optimized geometries of the zeo−OSDA−F systems is given in Figures 2 and 3.

Table 2. Predicted Zeolite Phase from Calculations (from Total Energies in Table 1) Compared to Experiments (from Figure 1)[a]

	F	F	noF	noF
SDA	predicted	experim.	predicted	experim.
sda01	AST	AST/NON	AST/NON	NON
sda02	MEL	MEL	MTW	MTW
sda03	STF	STF	STO	STO
sda04	STF	STF	STO	STO
sda05	STF	NES/CON/STF	STO	STO
sda06	DOH	DOH	STO	STO
sda07	CHA	CHA	CHA	MWW/CHA
sda08	LTA	LTA	UFI	UFI

[a]Predictions are taken from the lowest total energy for each SDA, both in fluoride (F) and nonfluoride (noF) media. For sda01, more than one phase is predicted (noF) because total energies for several zeolites are very close (within ±0.002 eV/SiO_2).

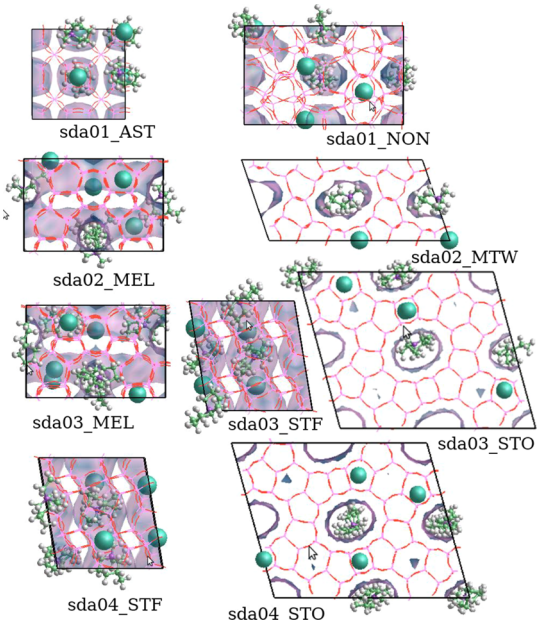

Figure 2. Calculated geometries of the systems zeo−OSDA−F with sdas 1−4 (see Figure 1). Fluoride anions are highlighted as large spheres.

Systems with **sda01** give some failures in the computational predictions. AST is correctly predicted as the stable phase in fluoride media, with a total energy lower than that for NON (−41.116 and −40.645 eV/SiO_2, respectively). NON has also been observed in fluoride media, and so both should give similar energies, contrary to the results. In fluoride-free media, calculations give very similar results for AST and NON (−40.571 and −40.572 eV/SiO_2), while only NON is experimentally reported.

Results of **sda02** indicate that MEL is the preferred phase in fluoride media because its total energy is lower than that for MTW (−40.754 and −40.736 eV/SiO_2). The differences are small but significant, since they refer to each SiO_2 unit, while

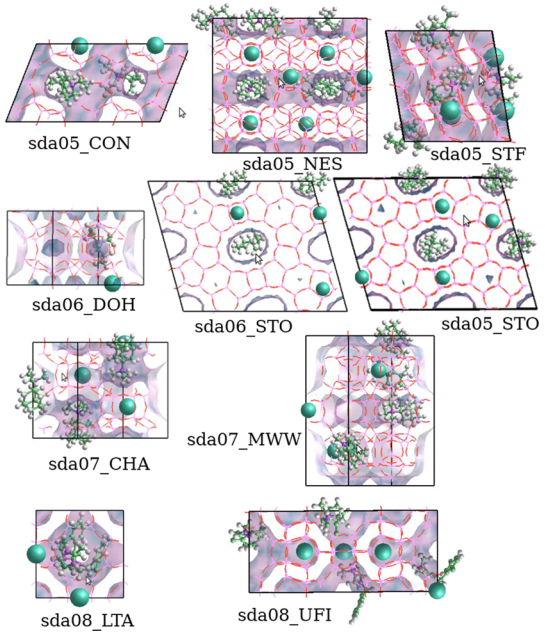

Figure 3. Calculated geometries of the systems zeo−OSDA−F with sdas 5−8 (see Figure 1). Fluoride anions are highlighted as large spheres.

for full unit cells, they become larger. In the absence of fluoride, the most stable phase becomes MTW, mainly driven by its larger framework stability. Both results are in agreement with experiments (Table 2). The fluoride energetic terms, (4) and (7) in Table 1, have a larger weight in MEL than in MTW, and this justifies why MEL is the product in fluoride media. MEL contains 4/96 OSDA−F molecules/SiO_2, a larger proportion than in MTW (2/56), hence contributing to the larger stability of the (4) and (7) contributions. Zeo−OSDA van der Waals interactions, per OSDA molecule, are more favorable for MTW than for MEL, with energies of −1.102 and −0.946 eV/OSDA, respectively, in fluoride-free media, and similar values in fluoride media. However, when taking into account the number of OSDA molecules per unit cell as well as the number of Si per unit cell, both contributions give the same value (−0.039 eV/SiO_2) in fluoride-free and very similar (−0.039 and −0.041 eV/SiO_2) with fluoride, meaning that the organic SDA is not driving the synthesis. This confirms the important role of fluoride as the SDA.

For **sda03**, two competing phases (STF; STO) were considered. With fluoride, STF is predicted, with the lowest total energy (−40.736 eV/SiO_2), in agreement with the experimental observation. The stability of STF in fluoride media is due to the large stability of the fluoride energetic terms, $E_{zeo-OSDAF}$ and E_{OSDAF}, (7) and (4) in Table 1, with values −0.314 and −0.175 eV/SiO_2, compared to −0.204 and −0.067 eV/SiO_2 (STO). Four [45^6] small cavities of STF are occupied by fluoride, giving a high packing efficiency contributing to the stability. The largest stability of STO in nonfluoride media is correctly predicted by the calculations giving −40.543 eV/SiO_2, compared to −40.491 eV/SiO_2 for STF. The structure-directing effect in fluoride-free media is not due to the organic SDA, which for STO shows the less stable zeo−OSDA van der Waals energy, −0.039 eV/SiO_2, but rather due to the framework stability, with STO being the most stable (Table S3).

https://doi.org/10.1021/acs.jpcc.1c08688
J. Phys. Chem. C 2022, 126, 2078−2087

For **sda04**, the competing phases are STF and STO. In fluoride media, STF, as with sda03, is the most stable (−40.782 versus −40.693 eV/SiO_2 for STO), while in fluoride-free media, STO is the most stable (−40.562 versus −40.512 eV/SiO_2 for STF); both results are in agreement with experiments. As in the previous case with sda03, the values of $E_{zeo-OSDAF}$ and E_{OSDAF} for STF (−0.313 and −0.173 eV/SiO_2) give much more stability than for STO (−0.189 and −0.094 eV/SiO_2). In hydroxide media, the role of the OSDA is not driving the synthesis: although the van der Waals shows more stability for STF (−0.069 eV/SiO_2) than for STO (−0.037 eV/SiO_2), the most stable phase is STO (E(z) in Table S3), in agreement with the experiments using sda03.

For **sda05**, a large number of zeolites (CON, NES, STF, and STO) compete, posing a challenge for the predictive capability of these methods. Calculations including fluoride predict STF as the product with the lowest energy, −40.775 eV/SiO_2, and with the more negative fluoride contributions, $E_{zeo-OSDAF}$ and E_{OSDAF} (−0.320 and −0.163 eV/SiO_2), in agreement with the experimental observation. When no fluoride is included in the calculations, STO is the zeolite predicted, with the lowest energy, −40.563 eV/SiO_2, compared to −40.502, −40.522, and −40.513 eV/SiO_2 for CON, NES, and STF, respectively. Although the most stable van der Waals zeo−OSDA interaction corresponds to STF, with −0.075 against −0.040 eV/SiO_2 for STO, once more the lower zeolite energy for STO (Table S3) drives the synthesis product.

STO also appears in the competition when using **sda06**, along with DOH, with the latter being dominant in the fluoride calculations and the former in fluoride-free media. STO appears in hydroxide media for the same reasons as above, hence not driven by zeo−OSDA van der Waals interactions but rather through zeolite stability. In the presence of fluoride, DOH is the preferred product by a very narrow difference, −40.670, compared to −40.668 eV/SiO_2 for STO.

CHA and MWW are the competing zeolite phases with **sda07**. With fluoride, CHA is the dominant product, with energy −40.871 compared to −40.662 eV/SiO_2 for MWW. The contributions $E_{zeo-OSDAF}$ and E_{OSDAF} provide a considerable stability (−0.325 and −0.276 eV/SiO_2, respectively). The latter term shows one of the most negative values of Table 1, indicating a large electrostatic SDA−F interaction, due to an effective packing (all cavities, for both the OSDA and fluoride, are fully occupied) between large cavities (where the OSDA is located) and small cavities (where fluoride is located). Without fluoride, also CHA is the product predicted, and experimentally observed, driven by a very stabilizing zeo−OSDA van der Waals energy, −0.115 (the most negative of all cases), compared to −0.049 eV/SiO_2 for MWW. Hence, this is a very effective OSDA for the synthesis of CHA. In hydroxide media, also MWW appears as the product, which is not predicted by the calculations, but the experiments show that this is achieved using a cotemplate (hexamethyleneimine).[46]

Finally, with **sda08**, LTA is the prediction using fluoride and UFI in hydroxide, in agreement with experiments. In fluoride, LTA provides the largest stabilization due to the $E_{zeo-OSDAF}$ and E_{OSDAF} terms, with −0.550 and −0.265 eV/SiO_2. The former value indicates a very effective interaction of the zeolite with both the OSDA and fluoride, due to full cavity occupation in both the OSDA and fluoride. In the absence of fluoride, both zeolites show a large van der Waals stabilization (−0.089 and −0.071 eV/SiO_2 for LTA and UFI), driving toward LTA, but the zeolite stability contributes to compensate this effect (−40.492 and −40.507 eV/SiO_2 for LTA and UFI, Table S3), giving a total energy lower for UFI (−40.407) than for LTA (−40.344 eV/SiO_2).

4. DISCUSSION

4.1. General Considerations of the Results in Fluoride Media. A total of 13 zeolite topologies have been explored in this study: AST, NON, MEL, MTW, STF, STO, CON, NES, DOH, CHA, MWW, LTA, and UFI. Of these, only three (AST, LTA, and UFI) contain D4Rs. As said above, fluoride is particularly useful to obtain pure silica zeolites but not necessarily containing D4Rs. The presence of small cavities, especially those containing 4-rings, facilitates the stability of fluoride. This is the case of the structures studied, which contain small cavities with 4-rings, as indicated in Table S5.

Overall, the results obtained in the presence of fluoride are not driven by the short-range zeo−SDA interaction but rather by two Coulombic terms, E(SDAF) and E(z-SDAF), in columns (4) and (7) of Table S4. The first term, E(SDAF), refers to electrostatic SDA^+−SDA^+, SDA^+−F^-, and F^-−F^- interactions, and by being a long-range energetic contribution, this refers to the ionic network of SDA^+ and F^- ions, that is, compatible with the zeolite micropores. Regarding the second term, E(z-SDAF) contains electrostatic zeo−SDA^+ and zeo−F^- contributions, with the electrostatic interaction between fluoride and the small cavity being particularly relevant.

The location of fluoride cannot be predicted based only on structural considerations. There is, so far, no evidence to support that the smaller the cavity is, the more stabilized the fluoride anions are. However, the values of E(z-SDAF) show the largest stability for sda01_AST, sda08_LTA, and sda08_UFI (Table S4), which are precisely the three structures containing D4Rs. Hence, this is a first hint that may allow one to establish an energetic criterion to rank the stability of small cavities containing fluoride anions.

The van der Waals zeo−SDA contribution, column (9), is relevant only for the synthesis of AST with **sda01** (−0.106 eV/SiO_2) and CHA with **sda07** (−0.114 eV/SiO_2). Sda01 is very specific to give pure silica AST but can also give other zeolites (LEV; ERI) in aluminosilicate gels, among other reasons because AST does not exist as aluminosilicate. Sda07 is acknowledged as the most specific SDA to obtain high silica[48] or pure silica CHA.[49] In the study by Muraoka et al.,[37] sda07 gives the lowest stabilization energy in CHA among a list of 20 OSDAs. High or pure silica is the condition that mostly enhances the role of the van der Waals zeo−SDA contribution, column (9) in Table S4, coming closer to what is known as "templating effect". However, there are always other contributions as we demonstrate in this study, and the current total energy decomposition contributes to a better analysis of energetic terms.

4.2. Water/Silica Ratio as a Synthesis Parameter in Fluoride Media. Two cases (sda01 and sda05) appear in Table 2 in which, experimentally, several phases are obtained in fluoride media, and they depend on the water/silica ratio of the synthesis gel. The general rule is that less-dense frameworks appear at lower water/silica and more-dense phases appear at larger water/silica ratios.[22]

When using pure silica and **sda01** in fluoride media, two zeolite phases can be obtained, AST and NON,[27] depending on the water/silica ratio. Typically, less-dense phases are obtained with more concentrated gels and this is the case for AST, while at larger water/silica, NON is the main product.

https://doi.org/10.1021/acs.jpcc.1c08688
J. Phys. Chem. C 2022, 126, 2078−2087

Reproducing these trends with calculations, or having a thermodynamic explanation of this behavior, is still beyond our current knowledge. Our results explain the reasons for the relative thermodynamic stability of the different phases. In the case of sda01, AST is more stable in fluoride media mainly due to two Coulombic terms, E(SDAF) and E(z-SDAF), in columns (4) and (7) of Table S4. This is related to the packing of cations (SDA^+) and anions (F^-) in the zeolite framework. Also, the van der Waals zeo−SDA contribution, column (9), is particularly favorable for AST and justifies in part its larger stability with respect to NON.

NES, CON, and STF are the zeolite phases obtained in fluoride media when using **sda05**. CON and STF (low and intermediate density) appear at low or intermediate water/silica, while NES (larger density) appears at large water/silica,[27] in agreement with the rule.[22] STF is the most stable according to our calculations. Once more, the two Coulombic terms, E(SDAF) and E(z-SDAF), are the main contributions that explain the larger stability of STF with respect to NES and CON. The van der Waals zeo−SDA term does not explain the zeolite phase obtained.

A previous study also highlighted the important role of the packing of SDA^+−F^- ions, which act as a subnetwork occluded inside the zeolite covalent microporous framework.[50] Apart from the well-known synthesis driving effects of zeolite stability and zeo−SDA interactions, the electrostatic SDA^+−F^- contribution was shown to play an important role in explanation of the zeolite formation. Among the number of small cavities available for fluoride location (a number larger than the number of fluoride anions), the occupied cavities could be explained by the distribution having the most stable Coulombic SDA^+−F^- contribution.

4.3. Presence of Defects as a Synthesis Parameter in Hydroxide Media. The positive charge of the SDA cannot be compensated by fluoride when the synthesis is made in hydroxide media, and this results in framework connectivity defects with negative charge. This negative charge comes from the so-called siloxy defects,[23,51,52] as indicated in Scheme 1.

Scheme 1. Siloxy Defect in a Zeolite (Right) and Framework without Defect (Left)

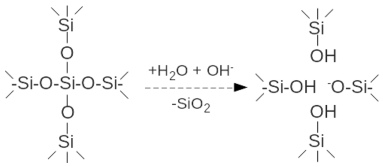

Hence, instead of our simple approximation of the neutral SDA, a more accurate way to model zeolite frameworks obtained in hydroxide media would be to generate one siloxy defect per each positive SDA charge. This includes considering a large number of combinations with the possible locations of the defects. Although they are expected to be close to the positive SDA charge, this is still a considerable challenge, similar to that of considering Al location/populations when the synthesis is made in aluminosilicate media. So far, according to the present results, even with this simplification, most of the computational results are in agreement with the experiments.

4.4. General Considerations of the Results in the Absence of Fluoride. As said above, the synthesis using pure silica gels in hydroxide media is the best condition to highlight the role of zeo−SDA interactions, whose main component is the van der Waals contribution, in column (9a) of Table S3. This contribution, by including all SDA molecules in the unit cell, also contains an effect of the zeolite porosity through the number of SDA molecules that can be occluded per SiO_2 unit. In order to check only the effect of zeo−SDA fitting, term (10) was also calculated.

A demonstration that even in the pure silica and nonfluoride conditions the zeo−SDA interactions are important but not determinant can be seen with **sda01** (Table S3). Columns (9a) and (10) show that the van der Waals zeo−SDA interactions are more favorable for AST, both in terms of SDA fitting, column (10), and also including the effect of porosity (number of SDA molecules per Si), column (9a), and in spite of this, AST is not preferred over NON, as shown by the virtually equal total energies (−40.571 and −40.572 eV/SiO_2, respectively). Factors such as the zeolite stability, E(z), SDA strain, column (2a), and a complex mixture of contributions, column (6a), are more favorable for NON than for AST and contribute to compensation of the lower energy of zeo−SDA interactions in AST.

Similarly, van der Waals zeo−SDA interactions are not dominant to drive the synthesis toward STO when using **sda03**, **sda04**, **sda05**, and **sda06**. Again, an inspection of the values in Table S3 indicates that the low energy of the zeolite, E(z), the small strain of the SDA, E(SDA) in column (2a), and the complex factor called E(SDA)(intra), column (6a), are the main contributions that give particularly large stability to STO when using these four SDAs. In none of these cases, E(z-SDA)(vdw) and E(z-sda)(vdw/SDA), columns (9a) and (10), show minimum values for STO, showing again that these syntheses are not driven by a strong template effect, and hence, SDAs are somehow reduced to the role of "pore fillers", as defined by Davis and Lobo.[53]

The role of the well-known trimethyl-adamantammonium (**sda07**) has been already discussed above, and the abundant literature shows that it is an excellent SDA to drive the synthesis to CHA. Due to the strong templating effect, with E(z-SDA)(vdw) = −0.114 eV/SiO_2 (Table S3), this selectivity is more pronounced when other factors such as the presence of defects and Al are not present, and therefore, CHA zeolites obtained with little Al or as pure silica are usually synthesized with sda07. The synthesis of not only CHA but also MWW in hydroxide and pure silica media using sda07 (see Figure 1) has been explained by the presence of organic fragments coming from the partial decomposition of sda07, which act as the cotemplate in the synthesis.[12] Hence, the computational result that does not predict the synthesis of MWW in the absence of fluoride (Tables 2 and S3) is fully justified.

The phase selectivity when using **sda08,** LTA in fluoride and UFI in hydroxyde media, with both zeolites containing the *lta* ($[4^{12}6^8 8^6]$) cavity, is a particularly interesting case. An important aspect is that in both zeolites, sda08 dimers are found in *lta* cavities. LTA and UFI contain D4R and *lta* cavities, but UFI, in addition, contains $[4^5 5^4 6^4 8]$ cavities, leading to a much larger distance between *lta* neighbor cavities in UFI than in LTA. UFI can then relax more efficiently *lta* cavities that are strained due to the presence of the large dimers occluded. This is the reason why sda08 molecules can relax better in UFI, as shown by the E(SDA) term, column (3a) (Table S3), lower in UFI than in LTA, and this is one of the main contributions that explains the larger stability of UFI in hydroxide media. Also, in the synthesis procedure,

https://doi.org/10.1021/acs.jpcc.1c08688
J. Phys. Chem. C 2022, 126, 2078−2087

tetramethylammonium cations were also needed as the cotemplate to obtain UFI,[46] and we attribute this to an additional stabilization of TMA cations inside $[4^5 5^4 6^4 8]$ cavities of UFI. When fluoride is present, the Coulombic terms E(SDAF) and E(z-SDAF), columns (4) and (7) in Table S4, give a larger stability to LTA, since *lta* and D4Rs are more efficiently packed and are closer to each other, without $[4^5 5^4 6^4 8]$ cavities present in UFI.

A comparison with the results of Schwalbe-Koda et al.[54] for some OSDAs employed in this work (Table S6 and Figure S1 of the Supporting Information) shows an apparent quantitative and qualitative disagreement in the values of E(z-sda)(vdw/SDA), although most of the calculated OSDA loadings in the zeolites are coincident. Examples of incorrect loadings in ref 54 are a single (instead of double) occupation of *lta* cavities in LTA and UFI by sda08, as well as the single occupation of sda07 in the MWW unit cell. A detailed comparison is beyond the aims of this study, but it is essential in order to benchmark and estimate the accuracy of the computational methods in predicting zeolite synthesis outcome.

A comparison with the results of zeo−OSDA pairs obtained by Jensen et al.[55] shows (Table S8) agreement for sda01, sda03, and sda08; a different set of results for sda07; and nothing reported for sda02, sda04, sda05, and sda06. The study provides an excellent literature extraction containing zeolite phase chemical composition, including the presence of fluoride, as well as OSDAs employed, which can be used for future studies.

5. CONCLUSIONS

Summarizing, subtle differences in the energetics of fluoride and fluoride-free calculations allow us to explain the preferred zeolite phase in each medium when using common OSDAs. Successful calculations of energetic stability have been possible due to (a) a sophisticated algorithm to automate the zeolite pore filled with both cationic OSDAs and fluoride, hence including accurate electrostatics; and (b) our accurate force field that includes all the components of the zeolite−OSDA−F models.

Not only organic and fluoride SDAs drive the synthesis, but also zeolite phase stability drives some synthesis products in hydroxide media, such as MTW (with sda02) and STO, in agreement with a previous study ranking stabilities of all-silica IZA zeolites.[56]

STO was obtained in hydroxide media with sda03, sda04, and sda05, in competition with STF, and with sda06 in competition with DOH. Although OSDAs were more stable in STF and DOH, the zeo−OSDA was not enough to compensate the effect of the zeolite framework stability, larger for STO. Selecting a better OSDA (with more negative zeo−SDA energy) would be needed in order to obtain STF in hydroxide media.

$E_{zeo-OSDAF}$ and E_{OSDAF} terms are rather constant for each zeolite regardless the OSDA, confirming the leading role of fluoride as the SDA, and allowing a fast and simple assessment for the overall stability in fluoride. Zeolites with large values of $E_{zeo-OSDAF}$ and E_{OSDAF}, with a major electrostatic component, are likely to be very stable in fluoride media, such as AST, STF, and CHA. The energetic analysis gives an explanation to the well-known stabilization of D4R-containing pure silica zeolite phases in the presence of fluoride, since the electrostatic $E_{zeo-OSDAF}$ contribution is the largest for zeolites containing D4Rs: AST, LTA, and UFI. Finally, the role of the OSDA through the van der Waals zeo−OSDA interactions is crucial in hydroxide media but not in fluoride.

■ ASSOCIATED CONTENT

Supporting Information

The Supporting Information is available free of charge at https://pubs.acs.org/doi/10.1021/acs.jpcc.1c08688.

Tables with data from all-silica zeolites and Ge-containing zeolites; further details of computational models and methods; further details of computational results, including tables with full details of energetic contributions in fluoride and fluoride-free systems; and comparison with recent work from the literature (PDF)

All optimized geometries of the zeo−OSDA−F systems (ZIP)

Tables with results of SciFinder search (PDF)

■ AUTHOR INFORMATION

Corresponding Author

German Sastre − *Instituto de Tecnologia Quimica UPV/CSIC, Universidad Politecnica de Valencia, 46022 Valencia, Spain*; orcid.org/0000-0003-0496-6331; Phone: +34963879445; Email: gsastre@itq.upv.es

Author

Santiago Leon − *Instituto de Tecnologia Quimica UPV/CSIC, Universidad Politecnica de Valencia, 46022 Valencia, Spain*

Complete contact information is available at: https://pubs.acs.org/10.1021/acs.jpcc.1c08688

Author Contributions

The manuscript was written through contributions of all authors.

Notes

The authors declare no competing financial interest.

■ ACKNOWLEDGMENTS

We thank MICINN of Spain for funding through projects RTI2018-101784-B-I00, RTI2018-101033-B-I00, and SEV-2016-0683. S.L. thanks MICINN for predoctoral grant BES-2017-081245 corresponding to project SEV-2016-0683-17-2. Prof. A. Corma is acknowledged for collaboration from the SEV-2016-0683 project. We thank ASIC-UPV for the use of computational facilities.

■ REFERENCES

(1) Flanigen, E. M.; Patton, R. L. Silica Polymorph and Process of Preparing Same. U. S. Patent 1978, 4, 073,865.

(2) Corma, A.; Navarro, M. T.; Rey, F.; Valencia, S. Synthesis of Pure Polymorph C of Beta Zeolite in a Fluoride-Free System. *Chem. Commun.* **2001**, *16*, 1486−1487.

(3) Corma, A.; Diaz-Cabañas, M. J.; Rey, F. Synthesis of ITQ-21 in OH− Media. *Chem. Commun.* **2003**, *9*, 1050−1051.

(4) Wagner, P.; Zones, S. I.; Davis, M. E.; Medrud, R. C. SSZ-35 and SSZ-44: Two Related Zeolites Containing Pores Circumscribed by Ten- and Eighteen-Membered Rings. *Angew. Chem., Int. Ed.* **1999**, *38*, 1269−1272.

(5) Schmidt, J. E.; Chen, C.-Y.; Brand, S. K.; Zones, S. I.; Davis, M. E. Facile Synthesis, Characterization, and Catalytic Behavior of a Large-Pore Zeolite with the IWV Framework. *Chem. − Eur. J.* **2016**, *22*, 4022−4029.

(6) Jackowski, A.; Zones, S. I.; Hwang, S.-J.; Burton, A. W. Diquaternary Ammmonium Compounds in Zeolite Synthesis: Cyclic

and Polycyclic N-heterocycles Connected by Methylene Chains. *J. Am. Chem. Soc.* **2009**, *131*, 1092−1100.
(7) Isaac, C.; Deroche, I.; Paillaud, J.-L.; Daou, T. J.; Ryzhikov, A.; Michelin, L.; Rigolet, S.; Josien, L.; Nouali, H. All-Silica SSZ-74 Synthesized in Fluoride or Fluoride-Free Media: Investigation on Organic Structure-Directing Agent's Locations Inside Pores. *Cryst. Growth Des.* **2021**, *21*, 4013−4022.
(8) Shinno, Y.; Iyoki, K.; Ohara, K.; Yanaba, Y.; Naraki, Y.; Okubo, T.; Wakihara, T. Toward Efficient Synthesis of Chiral Zeolites: A Rational Strategy for Fluoride-Free Synthesis of STW-Type Zeolite. *Angew. Chem. Int. Ed.* **2020**, *59*, 20099−20103.
(9) Gies, H. Studies on clathrasils IX Crystal Structure of Deca-dodecasil 3R, the Missing Link between Zeolites and Clathrasils. *Z. Krist.* **1986**, *175*, 93−104.
(10) Schlenker, J. L.; Rohrbaugh, W. J.; Chu, P.; Valyocsik, E. W.; Kokotailo, G. T. The Framework Topology of ZSM-48: A High Silica Zeolite. *Zeolites* **1985**, *5*, 355−358.
(11) Barrett, P. A.; Díaz-Cabañas, M. J.; Camblor, M. A.; Jones, R. H. Synthesis in Fluoride and Hydroxide Media and Structure of the Extra-Large Pore Pure Silica Zeolite CIT-5. *J. Chem. Soc., Faraday Trans.* **1998**, *94*, 2475−2481.
(12) Camblor, M. A.; Corma, A.; Díaz-Cabañas, M.-J.; Baerlocher, C. Synthesis and Structural Characterization of MWW Type Zeolite ITQ-1, the Pure Silica Analog of MCM-22 and SSZ-25. *J. Phys. Chem. B* **1998**, *102*, 44−51.
(13) Bialek, R.; Meier, W. M.; Davis, M.; Annen, M. J. The Synthesis and Structure of SSZ-24, the Silica Analog of AlPO4-5. *Zeolites* **1991**, *11*, 438−442.
(14) Lobo, R. F.; Tsapatsis, M.; Freyhardt, C. C.; Chan, I.; Chen, C.-Y.; Zones, S. I.; Davis, M. E. A Model for the Structure of the Large-Pore Zeolite SSZ-31. *J. Am. Chem. Soc.* **1997**, *119*, 3732−3744.
(15) Morris, S. A.; Bignami, G. P. M.; Tian, Y.; Navarro, M.; Firth, D. S.; Cejka, J.; Wheatley, P. S.; Dawson, D. M.; Slawinski, W. A.; Wragg, D. S.; et al. In Situ Solid-state NMR and XRD Studies of the ADOR Process and the Unusual Structure of Zeolite IPC-6. *Nat. Chem.* **2017**, *9*, 1012−1018.
(16) Wang, Y. X.; Gies, H.; Marler, B.; Müller, U. Synthesis and Crystal Structure of Zeolite RUB-41 Obtained as Calcination Product of a Layered Precursor: A Systematic Approach to a New Synthesis Route. *Chem. Mater.* **2005**, *17*, 43−49.
(17) Baerlocher, C.; Weber, T.; McCusker, L. B.; Palatinus, L.; Zones, S. I. Unraveling the Perplexing Structure of the Zeolite SSZ-57. *Science* **2011**, *333*, 1134−1137.
(18) Baerlocher, C.; McCusker, L. B.; Olson, D. H. *Atlas of Zeolite Framework Types*; 6th ed.; Elsevier: Amsterdam, 2007; http://www.iza-structure.org/databases
(19) Lu, P.; Villaescusa, L. A.; Camblor, M. A. Driving the Crystallization of Zeolites. *Chem. Record* **2018**, *18*, 713−723.
(20) Zicovich-Wilson, C. M.; San-Roman, M. L.; Camblor, M. A.; Pascale, F.; Durand-Niconoff, J. S. Structure, Vibrational Analysis, and Insights into Host-Guest Interactions in As-Synthesized Pure Silica ITQ-12 Zeolite by Periodic B3LYP Calculations. *J. Am. Chem. Soc.* **2007**, *129*, 11512−11523.
(21) Villaescusa, L. A.; Camblor, M. A. The Fluoride Route to New Zeolites. *Recent Res. Devel. Chem.* **2003**, *1*, 93−141.
(22) Camblor, M. A.; Villaescusa, L. A.; Diaz-Cabañas, M. J. Synthesis of All-Silica and High-Silica Molecular Sieves in Fluoride Media. *Top. Catal.* **1999**, *9*, 59−76.
(23) Liu, X.; Ravon, U.; Tuel, A. Evidence for $\overline{F}/Si\overline{O}$ Anion Exchange in the Framework of As-Synthesized All-Silica Zeolites. *Angew. Chem. Int. Ed.* **2011**, *50*, 5900−5903.
(24) Corma, A.; Rey, F.; Valencia, S.; Jorda, J. L.; Rius, J. A Zeolite with Interconnected 8-, 10- and 12-ring Pores and its Unique Catalytic Selectivity. *Nat. Mater.* **2003**, *2*, 493−497.
(25) Barrer, R. M. Stabilization of Lattices by Sorbed and Included Molecules. *J. Phys. Chem. Solids* **1960**, *16*, 84−89.
(26) Bell, R. G.; Lewis, D. W.; Voigt, P.; Freeman, C. M.; Thomas, J. M.; Catlow, C. R. A. Computer Modelling of Sorbates and Templates in Microporous Materials. *Stud. Surf. Sci. Catal.* **1994**, *84*, 2075−2082.
(27) Zones, S. I.; Burton, A. W.; Lee, G. S.; Olmstead, M. M. A Study of Piperidinium Structure-Directing Agents in the Synthesis of Silica Molecular Sieves under Fluoride-Based Conditions. *J. Am. Chem. Soc.* **2007**, *129*, 9066−9079.
(28) Sastre, G.; Leiva, S.; Sabater, M. J.; Gimenez, I.; Rey, F.; Valencia, S.; Corma, A. Computational and Experimental Approach to the Role of Structure-Directing Agents in the Synthesis of Zeolites: The Case of Cyclohexyl Alkyl Pyrrolidinium Salts in the Synthesis of *β*, EU-1, ZSM-11, and ZSM-12 Zeolites. *J. Phys. Chem. B* **2003**, *107*, 5432−5440.
(29) Sastre, G.; Cantin, A.; Diaz-Cabanas, M. J.; Corma, A. Searching Organic Structure Directing Agents for the Synthesis of Specific Zeolitic Structures: An Experimentally Tested Computational Study. *Chem. Mater.* **2005**, *17*, 545−552.
(30) Rojas, A.; Gomez-Hortiguela, L.; Camblor, M. A. Benzylimidazolium Cations as Zeolite Structure-Directing Agents. Differences in Performance Brought About by a Small Change in Size. *Dalton Trans.* **2013**, *42*, 2562−2571.
(31) Pophale, R.; Daeyaert, F.; Deem, M. W. Computational Prediction of Chemically Synthesizable Organic Structure Directing Agents for Zeolites. *J. Mater. Chem. A* **2013**, *1*, 6750−6760.
(32) Trachta, M.; Bludsky, O.; Cejka, J.; Morris, R. E.; Nachtigall, P. From Double-Four-Ring Germanosilicates to New Zeolites: In Silico Investigation. *ChemPhysChem* **2014**, *15*, 2972−2976.
(33) Turrina, A.; Garcia, R.; Cox, P. A.; Casci, J. L.; Wright, P. A. Retrosynthetic Co-Templating Method for the Preparation of Silicoaluminophosphate Molecular Sieves. *Chem. Mater.* **2016**, *28*, 4998−5012.
(34) Nimlos, C. T.; Hoffman, A. J.; Hur, Y. G.; Lee, B. J.; Di Iorio, J. R.; Hibbitts, D. D.; Gounder, R. Experimental and Theoretical Assessments of Aluminum Proximity in MFI Zeolites and its Alteration by Organic and Inorganic Structure-Directing Agents. *Chem. Mater.* **2020**, *32*, 9277−9298.
(35) Jo, D.; Hong, S. B. Targeted Synthesis of a Zeolite with Pre-established Framework Topology. *Angew. Chem. Int. Ed.* **2019**, *58*, 13845−13848.
(36) Fischer, M. Influence of Organic Structure-Directing Agents on Fluoride Dynamics in As-Synthesized Silicalite-1. *J. Phys. Chem. C* **2020**, *124*, 5690−5701.
(37) Muraoka, K.; Chaikittisilp, W.; Okubo, T. Multi-objective: De Novo Molecular Design of Organic Structure-Directing Agents for Zeolites Using Nature-Inspired Ant Colony Optimization. *Chem. Sci.* **2020**, *11*, 8214−8223.
(38) Schwalbe-Koda, D.; Gomez-Bombarelli, R. Benchmarking Binding Energy Calculations for Organic Structure-Directing Agents in Pure-Silica Zeolites. *J. Chem. Phys.* **2021**, *154*, 174109.
(39) SciFinder; Chemical Abstracts Service; https://scifinder.cas.org (accessed October 4, 2021)
(40) Gálvez-Llompart, M.; Cantín, A.; Rey, F.; Sastre, G. Computational screening of structure directing agents for the synthesis of zeolites. A simplified model. *Z. Krist. Cryst. Mater.* **2019**, *234*, 451−460.
(41) Burton, A. W.; Pradhan, A.; Sastre, G. Further investigations into "Zeolite Synthesis Using Flexible Diquaternary Alkylammonium Ions $(C_nH_{2n+1})_2HN^+(CH_2)_5N^+H(C_nH_{2n+1})_2$ with n = 1-5 as Structure-Directing Agents". *Microporous Mesoporous Mater.* **2006**, *95*, 366−371.
(42) Nakagawa, Y.; Lee, G. S.; Harris, T. V.; Yuen, L. T.; Zones, S. I. Guest/host Relationships in Zeolite Synthesis: Ring-Substituted Piperidines and the Remarkable Adamantane Mimicry by 1-azonio Spiro [5.5] Undecanes. *Microporous Mesoporous Mater.* **1998**, *22*, 69−85.
(43) Piccione, P. M.; Yang, S.; Navrotsky, A.; Davis, M. E. Thermodynamics of Pure-Silica Molecular Sieve Synthesis. *J. Phys. Chem. B* **2002**, *106*, 3629−3638.
(44) Eilertsen, E. A.; Arstad, B.; Svelle, S.; Lillerud, K. P. Single Parameter Synthesis of High Silica CHA Zeolites from Fluoride Media. *Microporous Mesoporous Mater.* **2012**, *153*, 94−99.

https://doi.org/10.1021/acs.jpcc.1c08688
J. Phys. Chem. C 2022, 126, 2078−2087

(45) Harris, T. V.; Zones, S. I. A Study of Guest/Host Energetics for the Synthesis of Cage Structures NON and CHA. *Studies Surf. Sci. Catal.* **1994**, *84*, 29−36.
(46) Jo, D.; Ryu, T.; Park, G. T.; Kim, P. S.; Kim, C. H.; Nam, I.-S.; Hong, S. B. Synthesis of High-Silica LTA and UFI Zeolites and NH3-SCR Performance of Their Copper-Exchanged Form. *ACS Catal.* **2016**, *6*, 2443−2447.
(47) O'Boyle, N. M.; Banck, M.; James, C. A.; Morley, C.; Vandermeersch, T.; Hutchison, G. R. Open Babel: An Open chemical Toolbox. *J. Cheminform.* **2011**, *3*, 33.
(48) Zones, S. I. Zeolite SSZ-13 and its method of preparation. US Patent 1985, 4544538.
(49) Diaz-Cabañas, M. J.; Barrett, P. A.; Camblor, M. A. Synthesis and structure of pure SiO2 chabazite: the SiO2 polymorph with the lowest framework density. *Chem. Commun.* **1998**, 1881.
(50) Pulido, A.; Corma, A.; Sastre, G. Computational Study of Location and Role of Fluoride in Zeolite Structures. *J. Phys. Chem. B* **2006**, *110*, 23951−23961.
(51) Dib, E.; Grand, J.; Mintova, S.; Fernandez, C. Structure-Directing Agent Governs the Location of Silanol Defects in Zeolites. *Chem. Mater.* **2015**, *27*, 7577−7579.
(52) Dib, E.; Grand, J.; Gedeon, A.; Mintova, S.; Fernandez, C. Control the position of framework defects in zeolites by changing the symmetry of organic structure directing agents. *Micropor. Mesopor. Mater.* **2021**, *315*, No. 110899.
(53) Davis, M. E.; Lobo, R. F. Zeolite and Molecular Sieve Synthesis. *Chem. Mater.* **1992**, *4*, 756−768.
(54) Schwalbe-Koda, D.; Kwon, S.; Paris, C.; Bello-Jurado, E.; Jensen, Z.; Olivetti, E.; Willhammar, T.; Corma, A.; Román-Leshkov, Y.; Moliner, M.; et al. A priori control of zeolite phase competition and intergrowth with high-throughput simulations. *Science* **2021**, *374*, 308−315.
(55) Jensen, Z.; Kwon, S.; Schwalbe-Koda, D.; Paris, C.; Gómez-Bombarelli, R.; Román-Leshkov, Y.; Corma, A.; Moliner, M.; Olivetti, E. A. Discovering Relationships between OSDAs and Zeolites through Data Mining and Generative Neural Networks. *ACS Central Sci.* **2021**, *7*, 858−867.
(56) Bushuev, Y. G.; Sastre, G. Feasibility of Pure Silica Zeolites. *J. Phys. Chem. C* **2010**, *114*, 19157−19168.

https://doi.org/10.1021/acs.jpcc.1c08688
J. Phys. Chem. C 2022, 126, 2078−2087